[30] A. A. Digeos, J. A. Valdez, K. E Sickafus, S. Atiq, R. W. Grimes, A. R. Boccaccini, *J. Mater. Sci*. **2003**, *38*, 1597.
[31] W. J. Weber, R. C. Ewing, *Science* **2000**, *289*, 2051.
[32] J. Nair, P. Nair, G. B. M. Doesburg, J. G. Van Ommen, J. R. H. Ross, A. J. Burggraaf, *J. Am. Ceram. Soc*. **1999**, *82*, 2066.
[33] R. Vassen, *J. Am. Ceram. Soc*. **2000**, *83* (8), 2023.
[34] J. M. Hermans, J. G. J. Peelen, R. Bei, *Ceram. Bull*. **2001**, *80*, 51.
[35] A. R. Boccaccini, M. Buecker, P. A. Trusty, M. Romero, J. M. Rincon, *Glass Technol*. **1997**, *38*, 128.
[36] I. Kravtchenko, V. Gorobinskaya, J. Bossert, *Mater. Eng*. **1999**, *10*, 193.
[37] J. Menciz, *Strength and Fracture of Glass and Ceramics*, Elsevier, Amsterdam **1992**.
[38] R. H. Doremus, *Glass Science*, 2nd edn., Wiley, New York **1994**.
[39] A. Rouanet, *Rev. Int. Hautes Temperatures et Refract*. **1971**, *8*, 161.
[40] P. Saewong, PhD Thesis, Imperial College, London **1998**, p. 45.
[41] W. Lutze, R. C. Ewing, eds. *Radioactive Waste Forms for the Future*, North Holland, Amsterdam **1988**.
[42] E. M. Rabinovich, *J. Mater. Sci*. **1976**, *11*, 925.
[43] S. S. Kim, J. G. Lee, I. K. Choi, G. H. Lee, K. S. Chun, *Radiochim. Acta* **1997**, *79*, 199.
[44] A. R. Boccaccini, P. A. Trusty, *J. Mater. Sci. Lett*. **1996**, *15*, 60.
[45] M. P. Borom, *J. Am. Ceram. Soc*. **1977**, *60*, 17.
[46] R. Chaim, V. Talanker, *J. Am. Ceram. Soc*. **1995**, *78*, 166.
[47] A. R. Boccaccini, *Ceram. Acta* **1996**, *8*, 5.

# Beneficial Effects of AlN as Sintering Aid on Microstructure and Mechanical Properties of Hot-pressed $ZrB_2$

By *Frederic Monteverde** and *Alida Bellosi*

Because of an excellent combination of thermomechanical, chemical and electrical properties, zirconium diboride ($ZrB_2$) has attracted much attention for its great potential to be widely used, such as in technically engineered ceramic. This ceramic is currently employed for instance as refractory in foundries, in electrical devices, nozzles, armour, or wherever high resistance to oxygen attack is required.[1] Moreover, $ZrB_2$ and, by extension, other borides like $HfB_2$ and $TaB_2$, could be used for ultra-high structural applications in aerospace.[2–6] Actually, competitive employment of these refractory borides is presently limited by their very low sinterability. The covalent nature of bonding demands the help of pressure-assisted sintering techniques at very high temperatures (>1900 °C) in inert atmosphere for obtaining highly dense pure bulks.[1] Excessive grain growth, originated by these extremely high sintering temperatures, often induces undesired microcracking and leads to detrimental effects on the mechanical properties.

The addition of nickel[7] or silicon nitride[8] as sintering aids has been proven to enhance the sinterability of $ZrB_2$ powders at processing temperatures below those needed for undoped $ZrB_2$, thus enabling the manufacture of highly dense components. The use of silicon nitride successfully conferred better mechanical properties,[9] in comparison to literature data for similar materials.[1,4,7] The primary role of the additive is ultimately the (partial) removal of the oxide layer that very often, covering the surface of the raw powders after mixing/milling processing, greatly limits the sinterability of ceramic borides.

The efforts to develop materials with economical and technical merits lead to the investigation of alternative doping systems. Therefore, the present work deals with the fabrication of a $ZrB_2$ bulk, hot-pressed at 1,850 °C with the addition of 4.6 vol.-% AlN as sintering aid. Microstructure and properties were studied and compared with those of an additive free $ZrB_2$.

*Fabrication of the Hot-pressed Material:* The selected commercial $ZrB_2$ powder (grade B, H.C. Starck, Germany) has a specific surface area of 1 $m^2/g$, and the particle size falls in the range 0.1–8 μm. The elemental impurities (from the company datasheet, wt.-%) are: O 1.0, C 0.25, N 0.25, Hf 0.2, Fe 0.1. The content of oxygen corresponds to 1.5 wt.-% of $B_2O_3$, due to surface oxidation of the powders during production and handling. The AlN powder (grade C, H.C. Starck, Germany), used as sintering aid, has a specific surface area of 4.3 $m^2/g$ and an oxygen content of 1.8 wt.-%.

The powder mixture, hereafter labelled ZBA, has the following starting composition (vol.-%): $ZrB_2$+4.6 AlN. It was homogenised for 24 hours in a polyethylene jar using ethanol and zirconia balls, dried with a rotary evaporator under a continuous stream of nitrogen, and finally sieved.

The powder mixture ZBA was then hot-pressed in low vacuum (0.5 mbar) at 1,850 °C for 30 minutes, with an applied pressure of 30 MPa using an induction-heated graphite die (internal and external diameter of 45 and 120 mm, respectively). The shrinkage of the green compact was measured during the hot-press run by recording the displacement of rams. The temperature (600 °C/h heating rate) was controlled by a pyrometer focused on the graphite die.

The final density was measured using the Archimedes method, while the relative density was estimated with the rule of mixture.

[*] *Dr. F. Monteverde, Dr. A. Bellosi*
*National Research Council,*
*Institute of Science and Technology for Ceramics*
*Via Granarolo 64, 48018 Faenza (RA), Italy*

[**] *This work was supported by ASI (Italian Space Agency) – Project NEIN 700257. The authors thank Dr. S. Guicciardi for the helpful discussion, and Mr. C. Melandri for the technical assistance on mechanical tests.*

  **DOI:** 10.1002/adem.200300349 

ADVANCED ENGINEERING MATERIALS



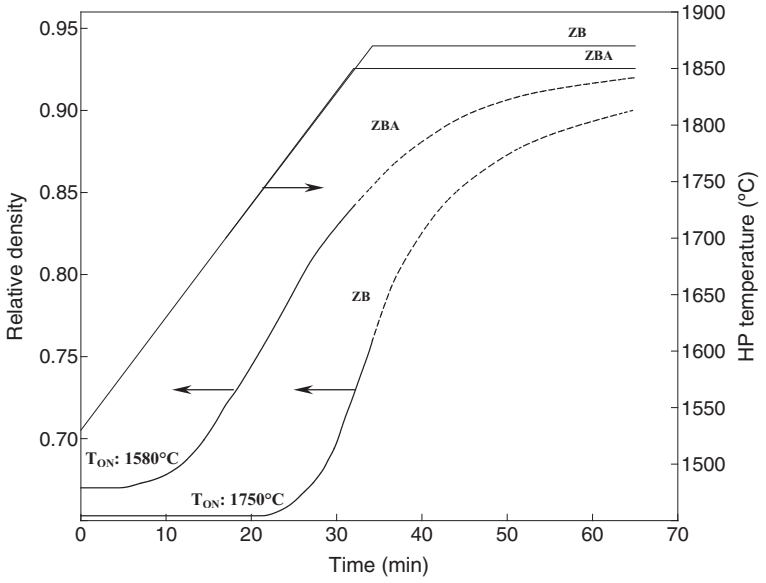


*Fig. 1. Relative density (left Y-axis) vs. time of material ZBA and ZB. The dotted portion of the hot pressing curves refers to the isothermal stage. Straight lines describe the hot pressing (HP) temperature schedule (right Y-axis).*

The microstructure was analysed with a scanning electron microscope (SEM, mod. S360, Cambridge, UK) equipped with an energy dispersive microanalyzer (EDX, mod. INCA Energy 300, Oxford Instruments, UK), and an X-ray diffractometer (XRD, mod. D500, Siemens, Germany).

Some thermodynamic calculations were performed using the HSC software package.[10]

*Properties of the Hot-pressed Material:* Young's modulus (E) was measured by the resonance frequency method on a 28.0 × 8.0 × 0.8 $mm^3$ plate. Flexural strength ($\sigma$) in a 4-pt. configuration was tested at room temperature and at high temperature (1,400 °C and 1,500 °C) in ambient air or flowing Argon, on 25.0 × 2.5 × 2.0 $mm^3$ chamfered bar (length x width x thickness, respectively), using 20 mm and 10 mm as outer and inner span, respectively, and a crosshead speed of 0.5 mm/min. The tests at high temperatures in flowing Argon were executed in a dedicated furnace (mod. HTTF, Severn Furnaces Ltd., UK). For each temperature and atmosphere, at least three bars were broken. Polished sections of the bars tested at high temperatures were prepared for SEM-EDX examination.

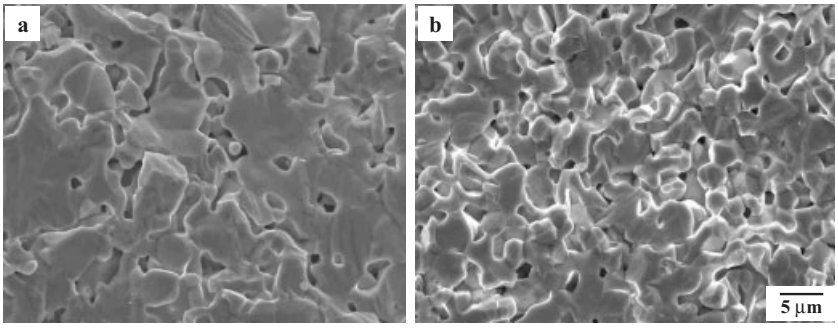


*Fig. 2. Secondary electron – SEM micrographs from fracture surface of material ZB (a) and ZBA (b).*

Microhardness (Hv1.0) was measured by a Vickers indenter with 9.81 N as applied load for 15 s on polished sections. Fracture toughness ($K_{ic}$) was evaluated using the chevron notched beam (CNB) method on 25.0 × 2.5 × 2.0 $mm^3$ bars (length × thickness × width, respectively) on the same jig used for the flexural strength with a crosshead speed of 0.05 mm/min.

The thermal expansion behavior was tested up to 1,350 °C in a stream of Argon (5 °C/min of heating rate). The electrical resistivity ($\rho$) was measured by a four probe d.c. method at room temperature, inducing a current along a 25.0 × 2.5 × 2.0 $mm^3$ bar.

Microstructure and properties of material ZBA were compared to an additive-free $ZrB_2$ (material ZB), hot-pressed at 1,870 °C for 30 minutes, under the same processing procedures described above.

*Densification Behavior during Hot-pressing and Microstructural Evolution:* The densification curves of material ZBA and ZB during the hot-press runs are displayed in Fig. 1. The final relative densities were evaluated at about 92 and 90 %, respectively. The temperature $T_{ON}$ (namely 1,580 and 1,750 °C for material ZBA and ZB, respectively) marks the onset of shrinkage of the green body during hot-pressing. However, in spite of very similar hot-pressing conditions, the final microstructure looks quite different. In particular, material ZB developed grains coarser than those of material ZBA (Fig. 2). In the former, excessive grain coarsening occurred, whereas the latter had a more modest grain growth with a predominance of equiaxed grains, and pores mostly located intergranularly. It follows that the addition of AlN in material ZBA played a fundamental role in modifying and activating densification mechanisms.

In both the studied materials, beside $ZrB_2$, XRD analyses did not detect any other crystalline phases. On the contrary, the SEM-EDX examination of a polished section of the as-sintered ZBA clearly identified small amount of secondary phases, namely residual AlN, $Al_2O_3$, and BN (Fig. 3). They are in the form of pockets, most often located at triple junctions of the $ZrB_2$ grains.

The formation of the mentioned reaction products can be explained on the basis of the chemical interaction between AlN and $B_2O_3$, precisely $2AlN + B_2O_3 = Al_2O_3 + 2BN$ (reaction 1). The $B_2O_3$ phase derives from the oxygen contamination upon the surface of the $ZrB_2$ particles. Reaction 1, characterized by negative Gibbs free energy (–270 kJ/mol at room temperature), is strongly favoured. It is therefore expected that the effect of the AlN addition during hot-pressing is to reduce the oxygen content of the $ZrB_2$ particles at relatively low temperatures, before significant shrinkage starts taking place (i.e. for temperature well below $T_{ON}$).

  

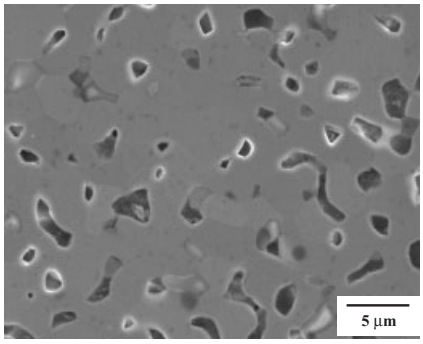


*Fig. 3. Secondary electron - SEM micrograph from a polished section of material ZBA.*

From this starting composition (wt.-%), 96.5 $ZrB_2$+ 1 $B_2O_3$+2.5 AlN, a multi-component equilibrium composition was calculated at 1,850 °C and 1 bar. On the basis of the final output (wt.-%), 96.5$ZrB_2$ + 1.5$Al_2O_3$ + 1.3AlN + 0.7BN, some important issues can be put forward:

– AlN interacts basically with oxygen-bearing species, i.e. boron oxide in our case
– $ZrB_2$ does not react with AlN, $Al_2O_3$ and BN.

These findings match properly with the SEM-EDX results described earlier.

It has been reported that the densification rate of $ZrB_2$ powder is highly sensitive to the boron activity.[11] The oxygen contamination has the effect of reducing boron activity through the production and volatilization of $B_2O_3$. The decrease in boron activity is accompanied by a reduction of the densification rate which, in turn, promotes grain coarsening by evaporation-condensation kinetics.

Although the difference in final density is rather limited, the grain size of the material ZB, having more residual oxygen on the particle powder (before important shrinkage begins, i.e. $T < T_{ON}$), turns out to be larger than that of material ZBA, which has a lower oxygen content. In the case of the hot-pressing procedure, the maximum attainable density is therefore strongly affected by the oxygen content and is severely limited by exaggerated grain growth.

The primary effect of the AlN addition is the depletion of the $ZrB_2$ particles from the outer oxide layer that prevents the obtainment of highly dense compacts. Similar behavior was already verified in pure $TiB_2$[12,13] or that doped with AlN.[14]

*Table 1. LTECs calculated in selected temperature ranges.*

| Material | LTEC ($10^{-6}$/°C) | | | |
|---|---|---|---|---|
| | (25–800)°C | (25–1000)°C | (25–1200)°C | (25–1350)°C |
| ZB | 7.05 | 7.55 | 7.5 | 7.5 |
| ZBA | 7.15 | 7.4 | 7.6 | 7.65 |

*Electrical and Thermomechanical Properties:* The experimental values of some properties are listed in Table 1 and 2. The relative dimensional change versus temperature is shown in Fig. 4 while the linear thermal expansion coefficients (LTEC) are listed in Table 1. For both the curves, the departure from linear behavior (up to 1,350 °C) is practically negligible.

Concerning the electrical resistivity, the $\rho$ value of material ZBA lies within the typical range of metals. The moderate improvement in relative density of material ZBA does not reflect an equivalent decrease in electrical resistivity because the amount of the residual porosity (8 vol.-%) is already below the threshold volume of the percolative model.[15] Moreover, the presence of a few percent of non-conductive compounds in material ZBA (i.e. $Al_2O_3$ and BN), has a negligible influence on the magnitude of the electrical resistivity.

In comparison to material ZB, the refinement of the grain size and the reduced amount of residual porosity represent the main microstructural features which both contribute to increase the microhardness of material ZBA.

Concerning the fracture toughness, the porosity is still responsible for the relatively low values of this property in both the materials. However, the contemporary occurrence of the inter-intra fracture mode of the $ZrB_2$ grains (Fig. 2) agrees with the results of a relatively higher value of $K_{LC}$ in the denser material ZBA.

In accordance with the best-fitting relationship calculated for monolithic $ZrB_2$ ($E/E_0 = \exp(-3.4p)$ with $E_0 = 539$ GPa and $p$ the volumetric porosity[9]), a value of $p = 0.08$ gives $E = 411$ GPa. This result agrees nicely with that experimentally measured for material ZBA (i.e. 407 GPa). The small discrepancy between these values of $E$ can be attributed to the presence of secondary phases like AlN, $Al_2O_3$ and BN having $E$ values lower than that of a $ZrB_2$ bulk free of secondary reaction products. In the case of material ZB, the higher content of residual porosity leads to a lower E value (346 GPa).

*Table 2. Experimental values of some properties of the hot pressed material: Young modulus (E), electrical resistivity (ρ), microhardness (Hv1.0), fracture toughness ($K_{Ic}$), flexural strength (σ).*

| Material | E (GPa) | ρ (μΩcm) | Hv1.0 (GPa) | $K_{Ic}$ (MPa$\sqrt{m}$) | σ (MPa) | | | | |
|---|---|---|---|---|---|---|---|---|---|
| | | | | | 25°C | 1400°C | | 1500°C | |
| | | | | | Air | Air | Ar | Air | Ar |
| ZBA | 407±5 | 24±1 | 9.4±0.5 | 3.1±0.5 | 580±80 | 300±20 | 360±20 | 200±5 | 360±30 |
| ZB | 346±4 | 15±1 | 8.7±0.4 | 2.3±0.2 | 350±30 | 210±20 | – | – | – |

  

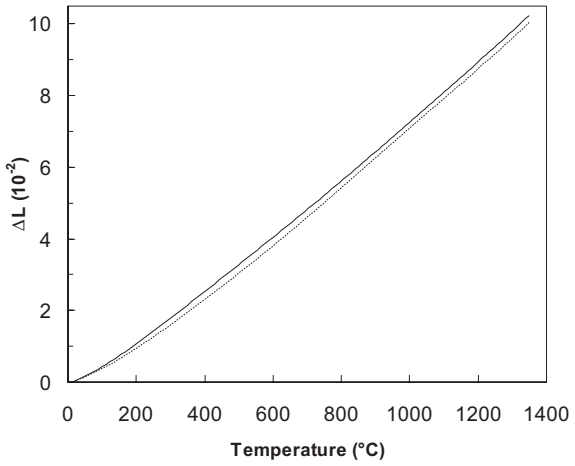


*Fig. 4. Relative dimensional change ΔL vs. temperature of material ZBA (full line) and ZB (dashed line).*

In comparison to material ZB, the increase in density and the obtainment of a finer grain size are mainly responsible for the improvement in flexural strength at room temperature of material ZBA. However, the scattering of the experimental values in material ZBA results larger than that in material ZB (Table 2). This is more likely due to the additional processing of the starting powder mixture (none for material ZB) that introduced a flaw population responsible for the enhanced dispersion of the strength measurements.

Concerning the tests at high temperatures, i.e. 1,400 °C and 1,500 °C in ambient air or flowing Argon, the results are very interesting and some general comments can be pointed out:

- the load vs. crosshead displacement curve, recorded during the flexural test, whatever the temperature or atmosphere, shows a linear behavior
- the oxidizing environment induces a decrease in flexural strength much steeper than that in a more protective atmosphere (i.e. Argon)
- the flexural strength in Argon at 1,400 °C and 1,500 °C are statistically undistinguishable
- the flexural strength measured in ambient air suffered a drastic drop from 1,400 °C to 1,500 °C.

The testing atmosphere greatly affects the high-temperature strength of material ZBA. Nonetheless, it should be highlighted the outstanding values of strength at such testing temperatures.

The microstructural SEM investigation on the polished cross-sections of the bars treated at high temperature in Argon (Fig. 5a,b) or ambient air (Fig. 5c,d) evidences the microstructural changes in material ZBA, depending on atmosphere and temperature. In contrast with the $ZrB_2$-Ni and $ZrB_2$-$Si_3N_4$ systems[7,9] the crucial finding about the linear elastic behavior up to 1,500 °C indicates that strength does not degrade due to the softening of grain boundary phases. To corroborate this hypothesis, no secondary phases which could significantly depress the overall stiffness of the material at high temperatures were found in material ZBA.

The main cause for the strength degradation apparently lies in the modified status of the surface of the flexural bar, before the test takes place. The contemporary action of temperature and atmosphere conditions could have changed the original flaw population in nature and size.

The microstructural modifications in the sub-surface of the tested specimens, shown in Fig. 5, confirm that the decrease in flexural strength is more pronounced for those samples which suffered a deeper alteration in their original microstructure (i.e. thicker external reaction layer). In fact, the bars tested in Argon at 1,400 °C and 1,500 °C, which exhibit an external reaction layer very similar in thickness and compactness (Fig. 5a,b), have a statistically undistinguishable mean value of strength (Table 2). The occurrence of the surface reaction scale, which is basically constituted by $ZrO_2$ particles, is mainly caused by a scarcely oxidizing atmosphere. It should be admitted that the sealing of the chamber in the HTTF furnace greatly abates the effects of an oxidizing environment, but does not reproduce a fully inert atmosphere.

On the contrary, the abrupt drop in flexural strength at 1,500 °C under air may be explained by the severe damage, in terms of a thicker and less compact $ZrO_2$-based scale, that the material ZBA experienced in such an oxidizing environment.

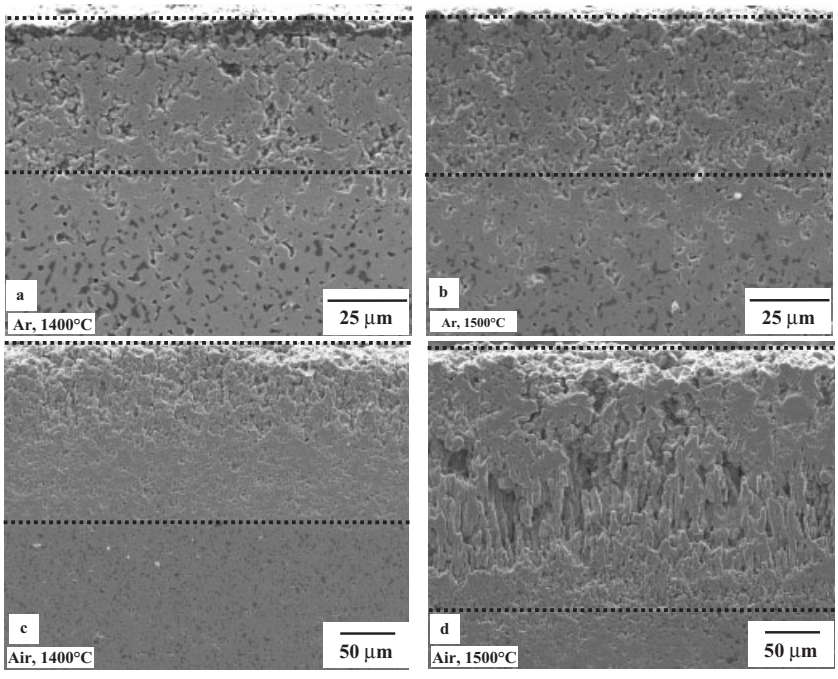


*Fig. 5. Secondary electron – SEM micrographs from polished cross section of material ZBA, tested in Argon at 1400°C (a) or 1500°C (b), and in ambient air at 1400°C (c) and 1500°C (d). The black horizontal lines indicate the $ZrO_2$ based layers that form in consequence of the material-environment interaction.*

  

The following conclusions can be drawn:

A monolithic $ZrB_2$ ceramic was hot-pressed at 1,870 °C for 30 minutes at low vacuum with the addition of 4.6 vol.-% of AlN as sintering aid, and a final relative density of 92 % was achieved.

In comparison with a pure $ZrB_2$ material, hot pressed at 1,870 °C for 30 minutes, the introduction of 4.6 vol.-% of AlN in the starting powder mixture greatly influenced the densification mechanisms. The additive-free material experienced excessive grain coarsening, whilst that doped with AlN, in spite of a very high hot-pressing temperature, had a more modest grain growth.

The primary effect of the AlN addition led to (partial) removal of the boron oxide layer that covers the $ZrB_2$ particles and prevents the achievement of dense sintered body. The refinement of the grain size and the presence of only refractory secondary phases like $Al_2O_3$ and BN had beneficial effects on the mechanical properties. In particular, outstanding strength values of 600 and 200 MPa were measured at 25 and 1,500 °C in ambient air, respectively.

*Received: January 30, 2003*
*Final: May 14, 2003*

[1] C. Mroz, *J. Am. Ceram. Soc. Bull.* **1995**, *74*, 164.
[2] S. R. Levine, E. J. Opila, M. C. Halbig, J. D. Kiser, M. Singh, J. A. Salem, *J. Eur. Ceram. Soc.* **2002**, *22*, 2757.
[3] C. R Wang, J.-M. Yang, W. Hoffman, *Mater. Chem. Phys.* **2002**, *74*, 272.
[4] M. M. Opeka, I. G. Talmy, E. J. Wuchina, J. A. Zaykoski, S. J. Causey, *J. Eur. Ceram. Soc.* **1999**, *19*, 2405.
[5] K. Upadhya, J.-M. Yang, W. P. Hoffman, *Amer. Ceram. Soc. Bull.* **1997**, *58*, 51.
[6] J. Bull, M.J. White, L. Kaufman, *US Patent 5,750,450*, **1998**.
[7] A. Bellosi, F. Monteverde, D. Dalle Fabbriche, C. Melandri, *J. Mater. Proc. Manufact. Sci.* **2000**, *9*, 156.
[8] F. Monteverde, A. Bellosi, *Scripta Mater.* **2002** *46*, 223.
[9] F. Monteverde, S. Guicciardi, A. Bellosi, *Mat. Sci. Eng. A* **2003**, *346*, 310.
[10] HSC Chemistry for Windows 5, Outokumpu Research Oy, Pori, Finland.
[11] D. N. Ovrebo, F. L. Riley, "Densification of zirconium diboride", Sixth Ecers Conference & Exhibition, Extended Abstract Vol.2, 19-20 (1999).
[12] S. Baik, P. F. Becker, *J. Am.Cer. Soc.* **1987**, *70*, 527.
[13] W. Wang, Z. Fu, H. Wang, R. Yuan, *J. Eur. Ceram. Soc.* **2002**, *22*, 1045.
[14] L-H Li, H-E Kim, E. S. Kang, *J. Eur. Ceram. Soc.* **2002**, *22*, 973.
[15] C. W. Nan, *Prog. Mater. Sci.* **1993**, *37*, 1.

# Unique Microcapsule Toner Synthesized by Liquid Phase Separation

By *Katsuya Teshima*

Curlfit is a unique technique developed for printing on three-dimensional objects with curved surfaces.[1] The desired image is printed onto a water-soluble film such as poly(vinyl alcohol), then the film is covered with acetate-containing solvents that act as an activator to dissolve the color. Subsequently, the film is floated in water in to which the object to be printed is then immersed. The design on the film is transferred to the surface of the object by water-pressure. At present, images for Curlfit are printed onto the water-soluble film by a gravure process. Curlfit printing has been applied to the manufacture of a wide variety of items, including decorative objects, sporting goods, automobile parts, and its applications continue to expand. Recently, on-demand printing of Curlfit designs has been strongly requested. Among on-demand printing methods, such as inkjet printing and digital printing used solid or liquid toners, the latter is most promising for Curlfit printing. A liquid toner is suitable for high-resolution printing since its particles are much smaller than those of a solid toner. Electrographic printers requiring special positively or negatively charged liquid toners with microencapsulated pigments, that is, microcapsule toners, are usually used for such on-demand printing.[2–6]

Various techniques are commonly used to synthesize such microcapsules,[7–14] including liquid phase separation, interfacial polymerization, solvent evaporation, and spray drying. Among these techniques, liquid phase separation (a physiochemical technique) is very convenient and can produce microcapsules even without water.[5] A microcapsule is a minute heterogeneous container that is usually either spherical when enclosing a fluid or roughly shaped when enclosing a solid, and generally consists of a core material enclosed with a wall material. In a liquid toner, microcapsules are dispersed in a non-polar solvent and charged either positively or negatively.

In this communication, we report the synthesis of a microcapsule toner for Curlfit printing by liquid phase separation in organic solvents. We have named this microcapsule toner "Curlfit toner". Various chemical and mechanical properties are required of this Curlfit toner. In particular, the wall material of the microcapsules is very important for the Curlfit toner. We, therefore, focus on the relationship between poly-

[*] *Dr. K. Teshima*
*Research & Development Center*
*Dai Nippon Printing Co., Ltd.*
*250-1 Wakashiba, Kashiwa 277-0871 (Japan)*
*teshima-k@mail.dnp.co.jp*

  **DOI:** 10.1002/adem.200300338 